ELSEVIER

Cretaceous Research 26 (2005) 283–297

CRETACEOUS RESEARCH

www.elsevier.com/locate/CretRes

A tsunami deposit at the Cretaceous/Paleogene boundary in the Neuquén Basin of Argentina

Roberto A. Scasso[a], Andrea Concheyro[a], Wolfgang Kiessling[b,*], Martin Aberhan[b], Lutz Hecht[c], Francisco A. Medina[a], Roald Tagle[c]

[a]*Departamento de Ciencias Geológicas, FCEN, Universidad de Buenos Aires, Ciudad Universitaria, Pab. 2, 1° Piso, 1428 Buenos Aires, Argentina*

[b]*Museum für Naturkunde, Institut für Paläontologie, Humboldt-Universität Berlin, Invalidenstr. 43, D-10115 Berlin, Germany*

[c]*Museum für Naturkunde, Institut für Mineralogie, Humboldt-Universität Berlin, Invalidenstr. 43, D-10115 Berlin, Germany*

Received 5 December 2003; accepted in revised form 21 December 2004

Available online 16 March 2005

Abstract

A coarse-grained sandstone bed of Cretaceous/Paleogene (K/Pg) boundary age occurs in a homogeneous neritic shelf mudstone sequence (Jagüel Formation) in the Neuquén Basin of Argentina. This bed, 15–25 cm thick, contains abundant plagioclase, broken shells and sharks' teeth. Sedimentological features include an erosive base, abundant rip-up clasts, normal grading and hummocky cross-bedding. The K/Pg boundary age of the bed was confirmed by calcareous nannofossils. Similar to other sections in the Gulf Coast region and the Danish Basin, a "dead zone" significantly depleted in macrofossils is evident in the basal 1 m above the clastic layer. In combination, these features suggest that the clastic layer represents a tsunami deposit that was related to the Chicxulub impact event in Yucatan/Mexico. Mechanisms of tsunami wave amplification in this extremely distal and somewhat protected setting are poorly understood but the funnel-shape of the basin may have promoted the unusually strong sedimentological response.

Keywords: Tsunami; Cretaceous/Paleogene boundary; Mass extinction; Patagonia; Argentina

1. Introduction

The global environmental consequences of large impacts are still poorly understood. Although it is now widely accepted that a major impact event in the Gulf of Mexico played a significant role in the end-Cretaceous mass extinction (Alvarez et al., 1980; Hildebrand et al., 1991), many details of the extinction mechanisms are still poorly resolved (Pope, 2002). Still open to discussion are the impact-caused environmental effects at regional versus global scales. In addition to global perturbations (wildfire, impact dust, sulphate aerosols), regional perturbations can be caused by shock waves, earthquakes, heat and tsunamis. Although marine extinction rates were globally nearly uniform (Raup and Jablonski, 1993; Kiessling and Baron-Szabo, 2004), ecosystem response was probably more heterogeneous (Schultz and D'Hondt, 1996; Kiessling and Claeys, 2001). To understand better regional ecosystem response and to separate regional from global perturbations, data on the geographic distribution of non-globally distributed impact tracers are crucial. Although the geographic patterns of shocked quartz distribution, tsunami and mass failure deposits are now reasonably clear for the Northern Hemisphere (Claeys et al., 2002), uncertainties

* Corresponding author.

E-mail address: wolfgang.kiessling@museum.hu-berlin.de (W. Kiessling).

0195-6671/$ - see front matter © 2005 Elsevier Ltd. All rights reserved.
doi:10.1016/j.cretres.2004.12.003

remain for the Southern Hemisphere. Just a few K/Pg boundary localities in the Southern Hemisphere have reported occurrences of shocked quartz, and reliable evidence of tsunami deposits has only been documented for the Pernambuco Basin in north-east Brazil (Albertão and Martins, 1996). Here we report new data on K/Pg boundary sections from the Neuquén Basin of Argentina where we have found evidence for a tsunami bed that is most likely related to the giant tsunami wave that originated at the Chicxulub impact site.

2. Geological setting

The Neuquén Basin is a foreland basin in western Argentina with a sedimentary record ranging from the Upper Triassic to Miocene. The Maastrichtian succession is transgressive whereas a general regressive trend is recorded in the Paleocene. The sea formed a narrow embayment to the west (Fig. 1), which gradually opened to the Atlantic Ocean to the east (Uliana and Biddle, 1988; Barrio, 1990). Marine deposits are recorded in the Jagüel Formation, a 90-m thick succession embracing the K/Pg boundary in the Neuquén Basin (Uliana and Dellapé, 1981). The Jagüel Formation consists of monotonous mudstones, which were deposited in a mid to outer shelf environment. It rests on a continental siliciclastic succession (Allen Formation) and is covered by bioclastic limestones of the Danian Roca Formation. An interval straddling the K/Pg boundary was previously defined palaeontologically based on foraminifers and calcareous nannofossils (Bertels, 1970; Náñez and Concheyro, 1997), ostracods (Bertels, 1975), and palynomorphs (Papú et al., 1999). The position of the K/Pg boundary is now constrained to a single, thin sandstone (Palamarczuk and Habib, 2001; Palamarczuk et al., 2002; this paper) in the upper half of the Jagüel Formation.

3. Data and methods

We have studied two sections: (1) Bajada del Jagüel (BJG, 38°6′S, 68°23′W) and (2) Opazo (OPZ, 38°8′S, 68°24′W), where the Jagüel Formation is best exposed (Fig. 2). Macropalaeontological data were gathered by taxon-quantitative sampling in defined stratigraphic intervals (20–50 cm near the boundary, 1–2 m at a

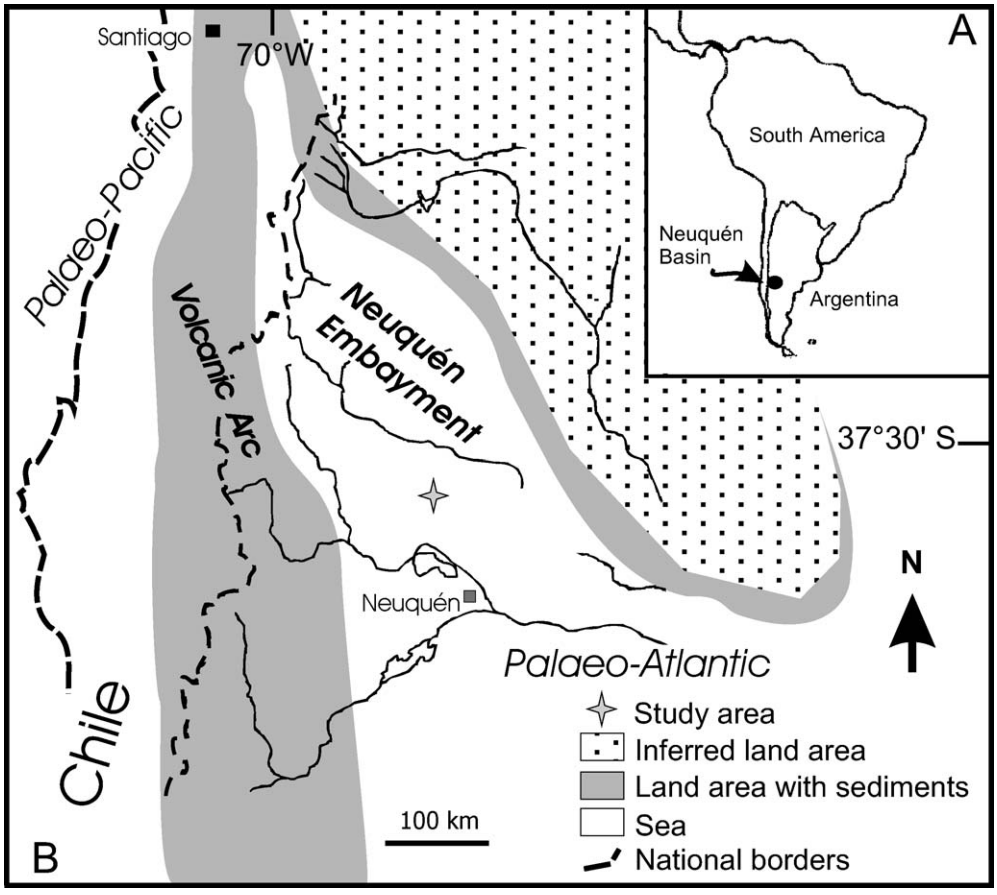

Fig. 1. A, map showing the location of the Neuquén Basin. B, palaeogeographic setting of the Neuquén Basin during the latest Cretaceous–earliest Paleocene (after Barrio, 1990). Study area: location of Bajada del Jagüel and Opazo sections.

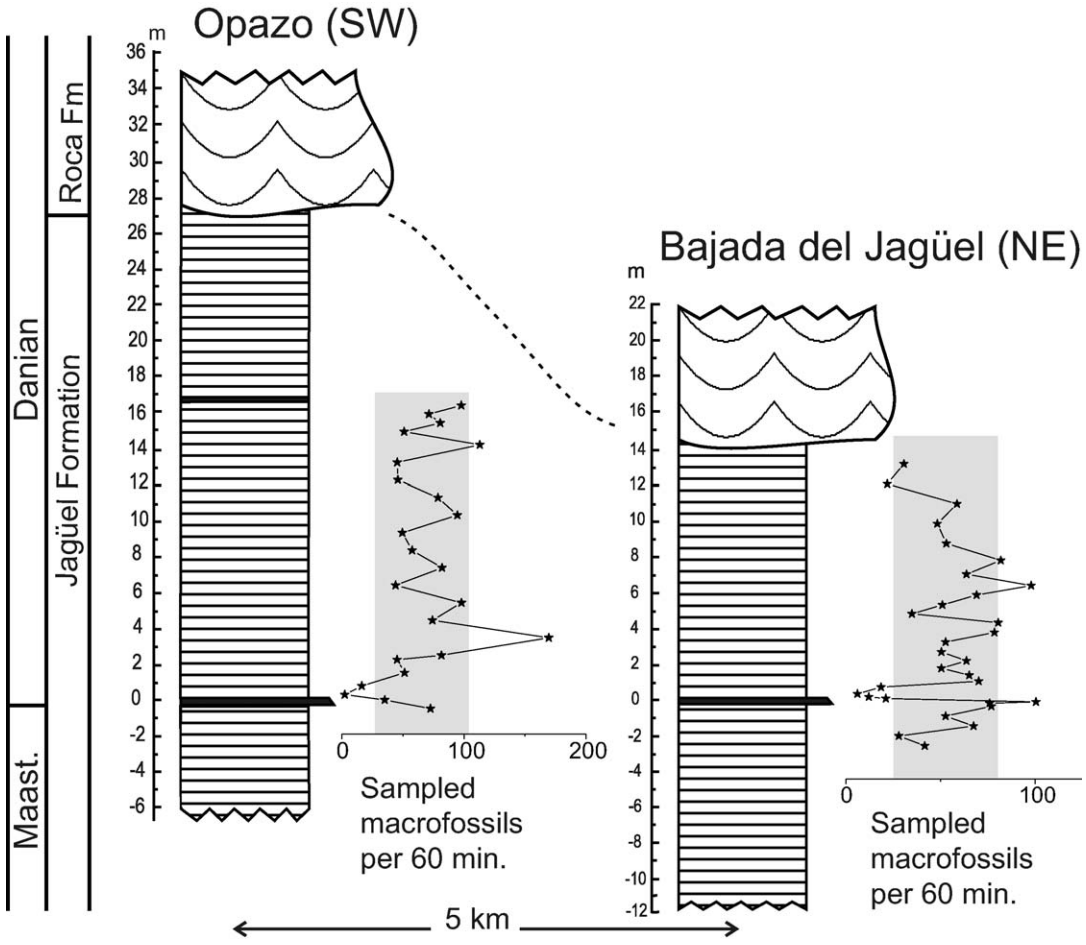

Fig. 2. Lithostratigraphic columns of, and macrofossil abundances in, the measured sections. Black bars indicate coarse-grained beds. The main sandstone beds coincide stratigraphically with the K/Pg boundary. Wavy pattern represents coarse bioclastic limestones of the Roca Formation. Grey shading in macrofossil abundance records (expressed as number of individuals) indicates one standard error around the mean value in both directions.

greater distance from it). Sampling effort was standardised by collection intensity (time of collecting, number of collectors). The number of individuals was determined according to standard procedures. In the case of disarticulated bivalves, the larger number of right or left valves was used.

In addition to macropalaeontological sampling, 14 samples were collected in a 1.1-m-thick microsection at Bajada del Jagüel for grain-size analysis and nannofossil examination. Additional samples were studied from intraclasts at the base of the sandstone bed (Figs. 3, 4) and orientated samples taken from the mudstone–sandstone contact. Smear slides were prepared following standard techniques (Bown and Young, 1998) and a semi-quantitative study has been carried out, examining at least two long slide traverses, corresponding to 300 fields of view.

Grain-size analyses were carried out by means of a Silas 1064 particle analyzer. Thins sections of sediments were studied under a standard petrographic microscope. An electron microprobe JEOL JXA 8800 was used for imaging, qualitative line scan analyses, and quantitative analyses of mineral composition. Quantitative analyses were calibrated using Smithsonian international mineral standards. The electron microprobe was operated at 15 kV and 15 nA and counting times were 20 s on peak and 10 s on background. The beam size was varied between <1, 3, and 10 μm. Large beam sizes of 10 μm were applied on fragile hydrous phases (e.g., glauconite). Whole-rock chemical analyses were carried out by X-ray fluorescence spectroscopy (XRF) with a SIEMENS SRS 3000 on glass tablets. For the tablets, 0.600 g of pulverized sample material, which was dried for four hours at 105 °C, 3.600 g of Di-lithiumtetraborate (BRA A10 Specflux), and, depending on the oxidation grade of the sample, approximately 0.5–2.0 g NH_4NO_3 for the oxidation of the sample material, were used. The concentration of platinum-group elements (PGE) was determined using ICP-MS in combination with nickel sulphide fire assay pre-concentrations

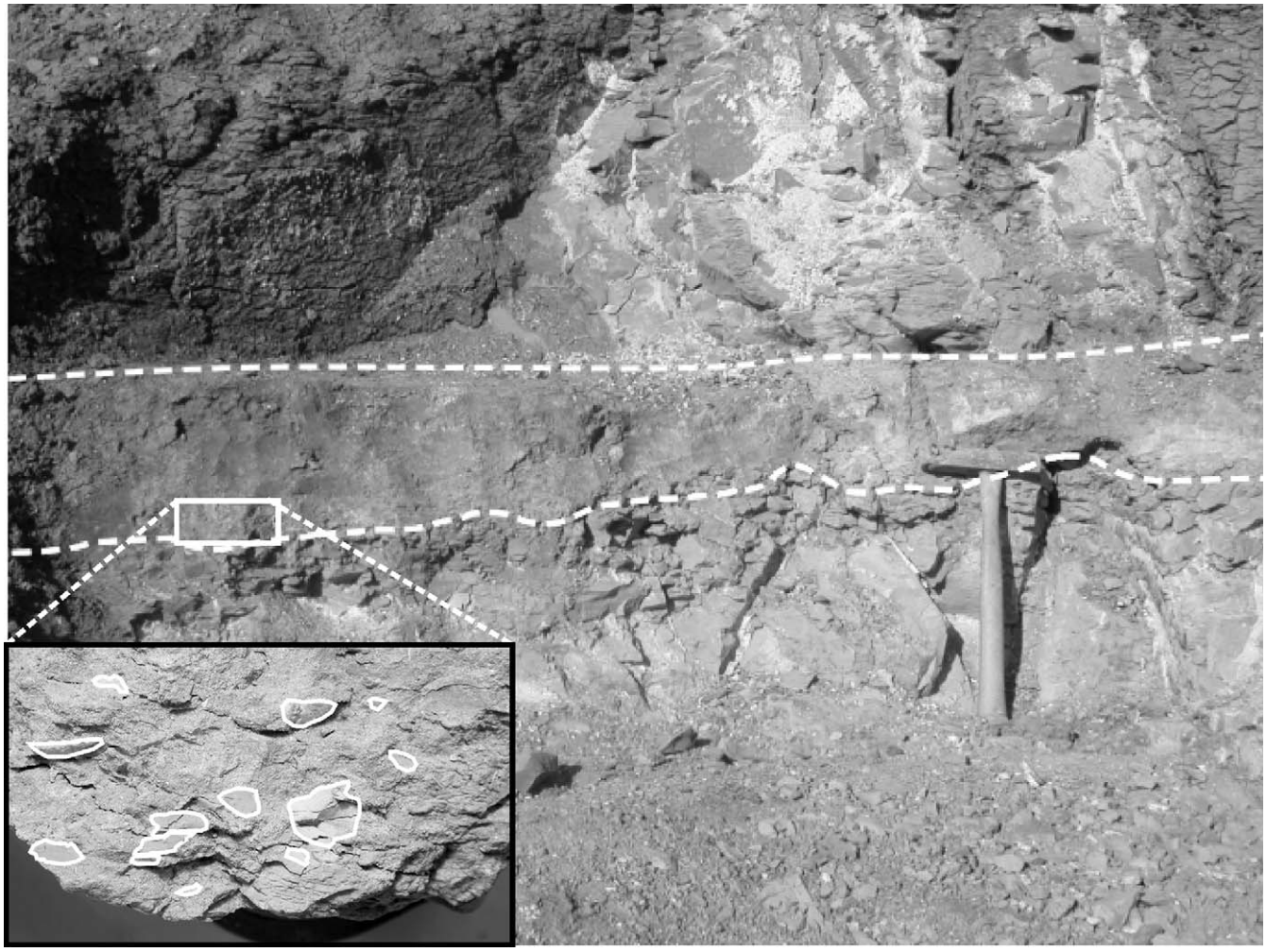

Fig. 3. Field photograph of the boundary layer at Baja del Jagüel. Erosive base and sharp upper contact indicated by dashed lines. Inset illustrates the coarse-grained lower part of the boundary layer and Maastrichtian intraclasts from underlying mudstones (outlined). Hammer shaft is 40 cm long.

(Plessen and Erzinger, 1998) that provides high precision down to concentrations of around 0.06 ng/g Ru, 0.01 ng/g Rh, 0.13 ng/g Pd, 0.04 ng/g Ir, 0.04 ng/g Pt and 0.09 ng/g Au.

4. Sedimentology and biostratigraphy

Massive, slightly consolidated silty mudstones dominate the sections. Mudstones are yellowish green in the Maastrichtian part and olive green in the Danian part. Bioturbation is poorly defined; recognisable forms are dominated by *Chondrites* and *Planolites*. However, the massive nature of the mudstones suggests intense bioturbation and a reasonably well-oxygenated environment. The depositional environment is interpreted as mid-shelf based on ratios of planktonic to benthic foraminifers (Bertels, 1975) and the presence of common pectinid bivalves. Accumulation took place below normal wave base. Storms are rarely recorded by thin shell concentrations, usually less than 2 cm thick, suggesting deposition close to storm wave base.

The BJG and OPZ sections contain a coarse-grained muddy sandstone bed, 15–25 cm thick (Fig. 3). Vertical, oblique and horizontal burrows 0.5–1 cm wide are abundant at the base of the sandstone layer (Figs. 4, 5). Burrows are filled with sand-sized plagioclase grains, sharks' teeth, and fragments of bivalves. Mudstones immediately above the sandstone bed are faintly laminated, and slightly coarser and darker than those beneath the bed. As will be discussed in the following paragraphs, this sandstone bed, based on evidence from calcareous nannoplankton, represents the K/Pg boundary in both sections. The occurrence of a thick sandstone layer is unique to both sections. Only the upper part of the OPZ section contains an additional unusual horizon, which is a strongly bioturbated, tuffaceous layer rich in biotite. This layer is discontinuous and absent in BJG, probably due to deep erosion prior to the deposition of the Roca Formation.

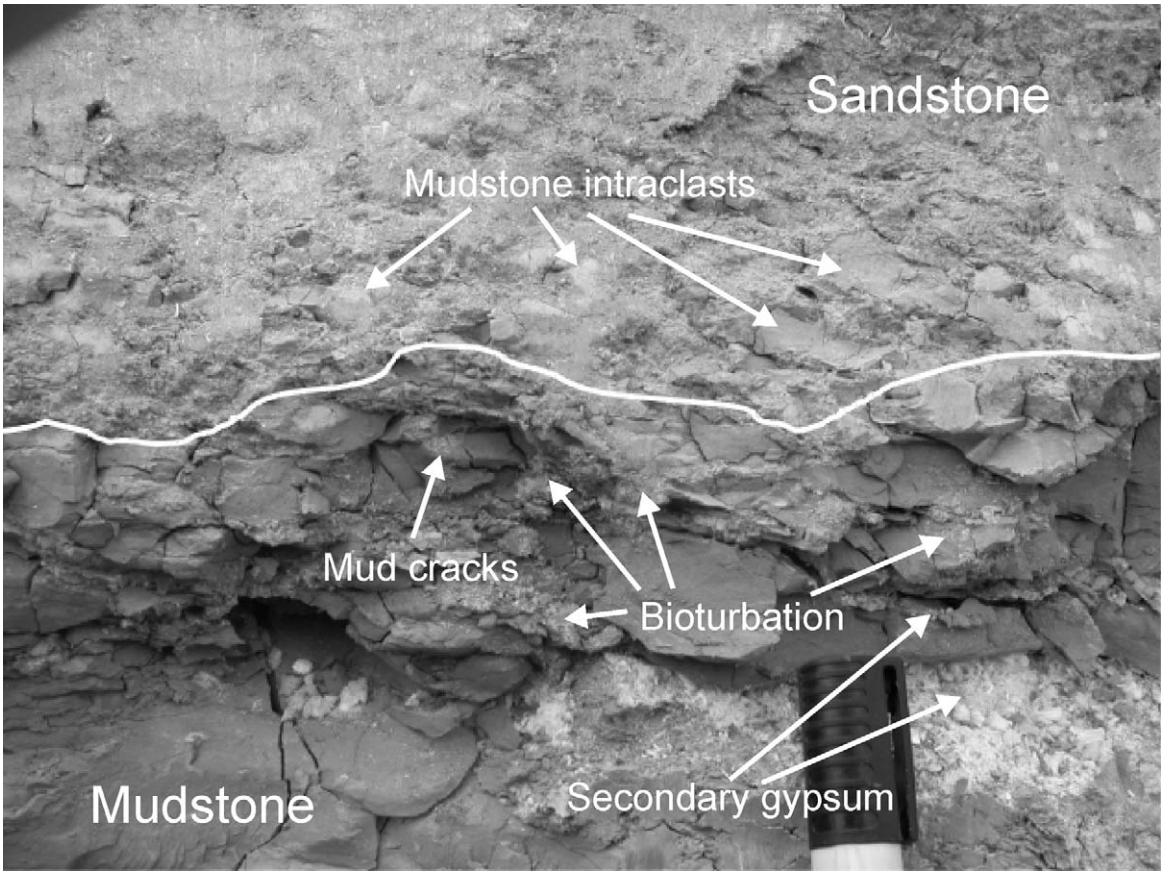

Fig. 4. Close-up of the base of the boundary layer showing burrows (ca. 0.5 cm in diameter; arrowed) extending from the boundary bed into the underlying mudstones. Width of pen is 2 cm.

A detailed analysis of calcareous nannofossils was performed at BJG to find the exact horizon of the K/Pg boundary and to detail the stratigraphic position of the sandstone bed (Table 1). Calcareous nannofossils comprise two well-differentiated associations. The first, located from the base of the section to the contact with the sandstone (samples BJ21–26), is Maastrichtian in age and characterized by *Arkhangelskiella cymbiformis*, *Cribrosphaerella daniae*, *C. ehrenbergii*, *Eiffelithus gorka*, *E. turriseiffeli*, *Kamptnerius magnificus, Micula decussata*, *M. murus*, *Nephrolithus frequens* and *Prediscosphaera stoveri* as the main representative species. The nannoflora is very diverse and common to abundant. Species preservation is moderate to good, without overgrowth effects.

The second association includes the sandstone bed to the top of the section sampled (samples BJ27–34), and is dominated by *Biantholithus sparsus*, *Cyclagelosphaera alta*, *C. reinhardtii*, *Markalius apertus*, *M. inversus*, *Micrantholithus pinguis*, *Neocrepidolithus cruciatus*, *N. neocrassus*, *Thoracosphaera operculata* and *T. saxea*, and is assigned to the Danian. The nannoflora is of low diversity and preservation varies from poor in the sandstone bed to moderate farther up the section. The first undoubted Danian nannofossils are noted in BJ29, in the upper half of the sandstone bed, where the two marker taxa of the first Cenozoic nannofossil zone (NP1 or NNTp1; Varol, 1998), *Biantholithus sparsus* and *Cyclagelosphaera alta*, have been found. An increase in abundance of survivor species such as *Thoracosphaera* spp. is already noted at the base of the sandstone bed, suggestive of an earliest Danian age for the whole bed. However, distinct blooms of *Thoracosphaera* or *Braarudosphaera*, seen in deposits of earliest Danian age in many other places (Kiessling and Claeys, 2001), are not evident in the BJG section. *Placozygus sigmoides*, the marker of subzone NNTp1B (Varol, 1998) is recorded in the first sample of mudstones overlying the boundary bed (BJ31) and in all samples above. NNTp2 (equivalent to the upper part of NP1) is first indicated in mudstones above the boundary bed in BJ32, by findings of *Cruciplacolithus primus*. Typical Cretaceous species, such as *Arkhangelskiella cymbiformis*, *Eiffellithus turriseiffelii* and *Micula decussata*, are rare in almost all of the Danian samples, with the general tendency towards fewer occurrences from BJ30 to the top of the section. The sequence of nannofossil extinctions and originations is comparable to that in many other sections globally (Jiang and Gartner, 1986; Henriksson, 1996; Pospichal, 1996; Gardin and Monechi, 1998).

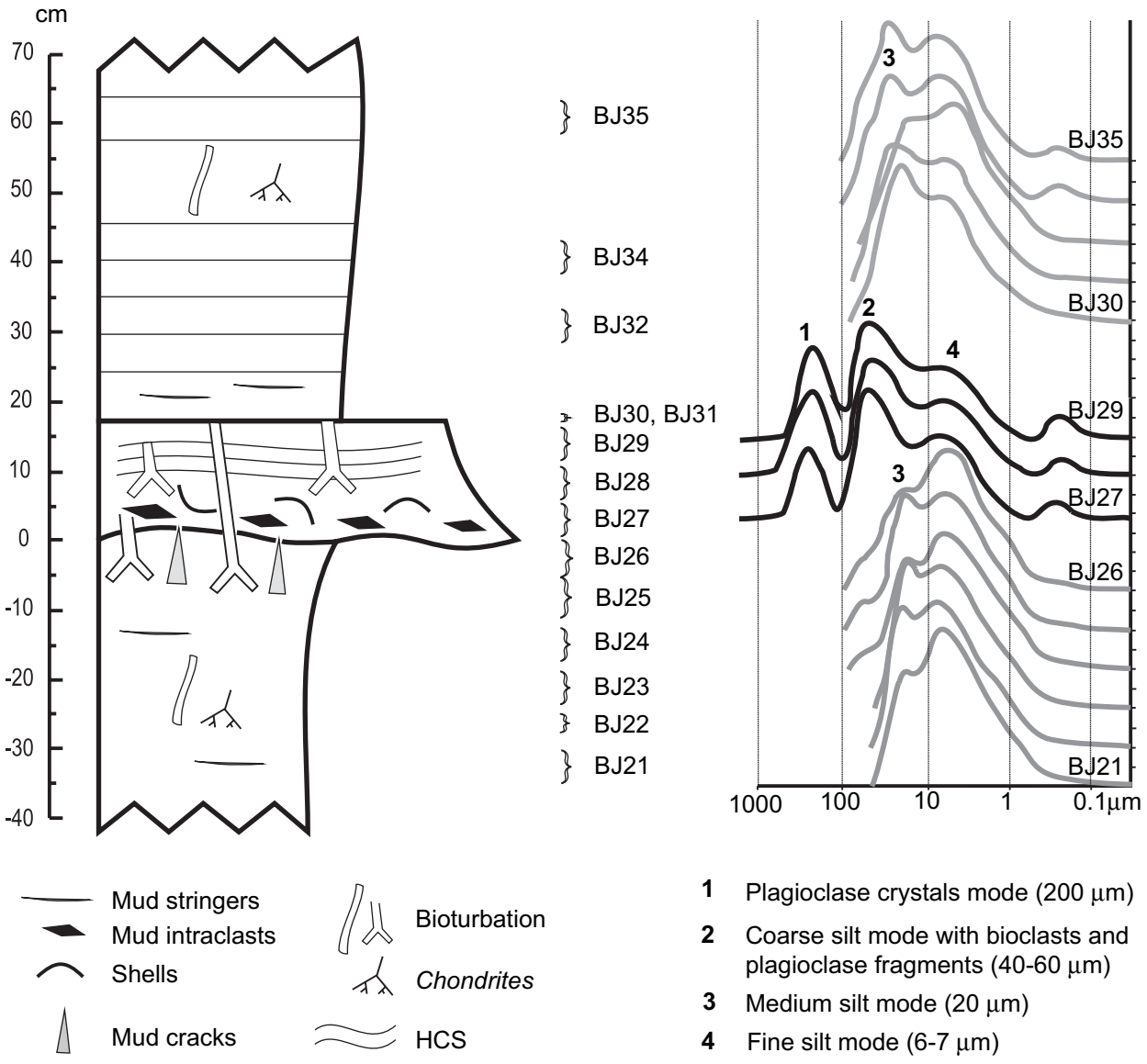

Fig. 5. Schematic section of the boundary interval. Sample numbers and grain-size distribution in the boundary layer and adjoining mudstones are indicated. The same sample numbers also refer to Table 1. The K/Pg boundary is placed at the base of the sandstone bed. HCS, hummocky cross stratification.

The K/Pg boundary is thus drawn at the base of the sandstone bed in both sections, confirming previous biostratigraphic studies (Concheyro and Náñez, 1994). Mudstone intraclasts in the boundary bed contain purely Maastrichtian nannofossils, but the matrix bears a predominantly Danian nannoflora. Danian assemblages are dominated by survivor nannoflora showing successive blooms identical to the pattern observed in cores from the North Sea (Varol, 1998).

5. Macrofossil distribution

Macrofossils are common and fairly well preserved throughout the section (Fig. 2). Bivalves dominate the assemblages, followed by gastropods and echinoids. Scleractinian corals were only observed in the Danian part of the section. Fossils are usually dispersed but are concentrated locally in thin coquinas and burrow fills. The abundance of macrobenthos, although fluctuating, is always above a certain threshold, with the exception of the mudstones immediately above the boundary bed. These are significantly depleted in macrofossils, only containing rare nuculids, ostreids and indeterminate bivalves, gastropods, and some echinoid spines. Macrofossil richness gradually increases up-section and reaches the "background" level (defined by the standard error of the mean abundance) 1 m above the sandstone layer. This pattern is similar to that described from other well-studied K/Pg boundary sections in Texas and

Table 1
Nannofossil distribution in the microsection studied at Bajada del Jagüel

STAGE	NANNOFOSSIL ZONES	SAMPLES	PRESERVATION	ABUNDANCE	Cretaceous Species																															Survivor Species											Cenozoic Species						Reworked Species		
					Actinozygus regularis	*Acuturris scotus*	*Ahmuellerella octoradiata*	*Arkhangelskiella cymbiformis*	*Biantholithus hughesi*	*Biscutum constans*	*Biscutum mealniae*	*Braarudosphaera bigelowi*	*Chiastozygus garrissoni*	*Cretarhabdus conicus*	*Cribrosphaerella daniae*	*Cribrosphaerella ehrenbergii*	*Eiffellithus gorkae*	*Eiffellithus parallelus*	*Eiffellithus turriseiffeli*	*Gartnerago segmentatum*	*Kamptnerius magnificus*	*Micula decussata*	*Micula murus*	*Nephrolithus frequens*	*Placozygus spiralis*	*Prediscosphera cretacea*	*Prediscosphaera spinosa*	*Prediscosphaera stoveri*	*Retecapsa crenulata*	*Rhagodiscus angustus*	*Rhagodiscus reniformis*	*Staurolithites melinciensis*	*Stradnerlithus snyderi*	*Vagalapilla aachena*	*Watznaueria barnesae*	*Acanthoica sp.*	*Braarudosphaera discula*	*Chiastozygus ultimus*	*Cyclagelosphera reinhardtii*	*Markalius inversus*	*Neochiastozygus primitivus*	*Neocrepidolithus cruciatus*	*Neocrepidolithus neocrassus*	*Thoracosphaera crassa*	*Thoracosphaera operculata*	*Thoracosphaera saxea*	*Biantholithus sparsus*	*Cruciplacolithus primus*	*Cyclagelosphaera alta*	*Markalius apertus*	*Micrantholithus pinguis*	*Placozygus sigmoides*	*Micrantholithus hoschulzii*	*Micrantholithus obtusus*	*Nannoconus bucheri*
DANIAN	NNTp2	BJ34	M	R				R			R	R				R					R	R			R										R				R	R		R	R		R	R	R				R	R			
		BJ33	M	F	R		R															R			R	R														R			R	R	F	F	R			R	R	F			
		BJ32	M	F								R				R			R			R													R	R			R	R	R		R	R	R	F		R			R	R			
	NNTp1	BJ31	M	R				R		R						R			R																R	R				R	R	R	R		F	R			R	R		R	R	R	R
		BJ30	M	F								R					R		F			F																		R			R		R	R									
		BJ29	M	R				R														R																		R			R		R		R		R	R					
		BJ28	M	R				R														R																		R			R		R	R									
		BJ27	M	C		R		F							R		F		F	R	R	C	R	R	R						R						R	R					R		R										
MAASTR.	UC20	BJ26	M	C				F							R	R	F		F	F		C		R	R			R		R	F	R			R				R						R										
		BJ25	M	C	R		R	F				R	R				R			R	R	C			R	R		F			R	R			R					R															
		BJ24	M	C			R	F				R		R	R	F		R	F	R	R	C			R	R				F	R	R	R		R																				
		BJ23	G	A			R	C				R	R		R	F	R		C	R	R	A	R	R	R			F		R	R		R		R																				
		BJ22	G	A	R	R		C					R	R	R		F	R	C	R	R			R	R	R		F		F	R	R		R																					
		BJ21	M	A	R	R		C	R				R		R	F	F	R	F	R	F	A			R	R	R	F	R	R	R	R			R																				

Nannofossil zones according to Burnett (1998) and Varol (1998). Sample labels as indicated in Fig. 5. Shaded sample labels are from the sandstone bed.
Preservation: M, moderate; G, good. Abundance: R, rare; C, common; F, frequent; A, abundant.

Denmark (Hansen et al., 1993; Håkansson and Thomsen, 1999), and we similarly interpret this fossil-poor interval as a "dead zone" caused by sudden ecosystem collapse and biomass decline. Macrofossils in the sandstone layer are common, and dominated by the pterioid bivalve genus *Entolium*. All macrobenthic taxa recorded from the sandstone layer were also found in the underlying mudstones, but several of them appear to be absent from the mudstones above. Given the K/Pg boundary age of the sandstone bed (based on the nannofossil assemblages) we interpret the sandstone macrofauna to represent reworked Maastrichtian elements.

6. Boundary bed

The sandstone bed of K/Pg boundary age (boundary bed) is an unconsolidated to slightly consolidated, strongly mottled, muddy sandstone. Although exhibiting pronounced pinch and swell (Fig. 3), the bed can be traced laterally for 5 km in the area. The sandstone is strongly dominated by subhedral plagioclase (90% of the sand fraction). The crystals are often broken and show angular to slightly rounded outlines (Fig. 6A, C, G). Other components of the sand fraction are glauconite aggregates (often oxidized; Fig. 6A), volcanic lithics (Fig. 6B), quartz, albite, iron oxides, mudstone intraclasts, mollusc fragments (Fig. 6D), echinoid spines (Fig. 6B), foraminifers (Fig. 6G) and ostracods.

The boundary bed is normally graded due to the concentration of mudstone intraclasts and larger shells at the base of the bed. Although it is intensely bioturbated, there are traces of hummocky cross-bedding in its upper part. Elongated, angular mudstone intraclasts with nannofossils of Maastrichtian age, up to 3 cm in longest diameter, are abundant at the erosive base. Macrofossils are most common in the lower half of the bed. Polymodal grain-size distribution point to mixing of several lognormal populations of particles, related to the varied origin of the materials (Fig. 5). Concentration of coarse materials in a sandy-plagioclase mode of about 200 μm is consistent with a distal, explosive volcanic origin for the plagioclase crystals (e.g., Carey and Sigurdsson, 2000).

Oscillatory zoning is common in plagioclase clasts. Qualitative line scan analyses (Ca-Kα peak) of a zoned plagioclase grain revealed a rather steep core to rim increase of the anorthite component from low towards high anorthite zones (Fig. 7A, B). Irregular undulatory growth zones indicate stages of plagioclase resorption (Fig. 7A). Growth zones are locally lined by primary fluid or melt inclusions. These zonation patterns are typical for plagioclase growth in an evolving subvolcanic magma chamber that is repeatedly recharged by hotter and more mafic (basaltic) magma before eruption (Shelly, 1993). Except for some rare albite grains that occur in the clastic matrix, the anorthite component of plagioclase clasts and plagioclase microphenocrysts in lithic clasts ranges between An_{50} to An_{73}, which is mainly labradorite (Fig. 7C). Although labradorite and bytownite are typical plagioclase of basaltic rocks, phenocrysts with strong oscillatory zonation, typical for andesitic rocks, commonly also show such high anorthite contents. Plagioclase is unaltered in most cases. In some plagioclase grains, however, anorthite-rich cores or growth zones are replaced by analcime, calcite or gypsum (Fig. 6E, H). In one case a plagioclase core is replaced by Sr-rich barite.

Two types of lithic clasts were observed in the matrix. One type is mainly composed of a very fine grained quartz and feldspar matrix (Type L in Fig. 6E, H). This clast type locally contains euhedral to subhedral plagioclase microphenocrysts (Fig. 6H), whereas the matrix grains are unhedral. Quartz in the matrix shows corrosion by feldspar. The other lithic clast type is characterized by acicular plagioclase microphenocrysts embedded in a matrix with a vesicular texture (type g in Fig. 6E). Larger vesicles (10–30 μm) are generally filled by secondary minerals such as analcime (Fig. 6F). The matrix of this clast type has a micro-porosity with pore diameters of less than 1 μm. We suggest that this clast type represents glass shards from an explosive eruption of a volatile-rich magma.

No impact tracers such as spherules, shocked quartz or an enrichment of a meteoritic component were found in the boundary bed, or in the mudstones immediately above the boundary bed. The PGE concentrations are mostly below the detection limit and below the values of the average continental crust proposed by Peucker-Ehrenbrink and Jahn (2001). Furthermore, the PGE patterns of the two samples conform to the fractionated PGE pattern of continental crust.

7. Origin of the boundary bed

Sedimentation around the K/Pg boundary in Neuquén took place below normal, fair-weather wave base in a shallow shelf, epeiric sea, which opened to the South Atlantic Ocean in the south-east. The co-occurrence of tempestites, seismites, and tsunamiites should be considered normal in this type of setting (Pratt, 2002), especially if there was tectonic activity close to or in the basin, as reported from Neuquén (Barrio, 1990). The bed at the K/Pg boundary shows several characteristics, such as bed thickness, erosive base, coarse grain-size, normal grading and hummocky cross-bedding that can be either attributed to a storm or tsunami deposit in a shelf environment (Hayes, 1967; Aigner, 1985; Bourgeois et al., 1988; Snedden and Nummedal, 1991;

Cheel and Leckie, 1993; Molina et al., 1997; Pratt, 2002). Distinction between tsunamites and tempestites is difficult, even in recent deposits close to the coastline (Nelson et al., 1996; Bondevik et al., 1997; Dawson, 1999; Clague et al., 2000; Nanayama et al., 2000; Goff et al., 2001; Peters et al., 2003), and very little is known about tsunami deposits in the offshore shelf. Most studies from shelf interiors refer to ancient deposits (Pratt, 2002), some of them related to the tsunami generated by a bolide impact at the K/Pg boundary (Bourgeois et al., 1988; Smit et al., 1992; Albertão and Martins, 1996).

Normal, background sedimentation in Neuquén is represented by silty muds deposited from suspension, and only big storms left their imprint in the form of rare, thin ($\leq$2 cm), sharp-based and normally-graded concentrations of shells typical of distal tempestites (Aigner, 1985). The boundary layer is unique in the entire sequence, because it is thicker and coarser grained than the tempestites, and because its sedimentary structures and composition are different. Mudstone intraclasts and other intra-basinal components such as foraminifers, shell fragments, echinoid spines, glauconite, sharks' teeth and other phosphate remains, concentrated in the lower part of the bed, together with the irregular, erosive base, suggest scouring of the sea floor and winnowing of fines before deposition of the heavy, coarse particles.

Plagioclase, bioclasts and intraclasts are of autochthonous or parautochthonous origin, and the intraclasts within the sandstone bed clearly stem from the underlying mudstones. Hummocky cross-stratification points to the action of oscillatory flows. These observations, together with the absence of allochthonous particles, suggest that the intraclasts were eroded and reworked in situ by oscillating currents from wave action (Mount and Kidder, 1993; Pratt, 2002).

The intra-basinal nature of the deposit points to a very unusual event for the origin of the deposit. In addition, the high concentration of macrofossils and other coarse particles suggests that: (1) during heterogeneous liquefaction of mudstones, combined flows winnowed the sea floor producing an irregular surface; (2) the liquified muds on top were also partly winnowed (Seguret et al., 2001), and sand-sized and coarser particles were concentrated; and (3) the sea floor was finally covered with bioclasts, intraclasts, sand and silt of autochthonous or parautochthonous origin. The top of the underlying mudstones is partially disrupted but still displays a geometrical fit (jigsaw structures) interpreted as a product of partial (heterogeneous) liquefaction of the sea floor induced by wave-cycling loading (e.g. Bouchette et al., 2001) on partially cohesive muds. Cracks were produced either by wave loading when the first tsunami wave struck the basin, or by differential mechanical behaviour of stiff mud underlying loose sand (Cowan and James, 1992) under the stress of the secondary waves (seiches). Sharp contacts at the base and top of the bed, well-preserved shells lacking bioerosion and biogenic crusts, the angularity and size of the intraclasts, and the lack of compound intraclasts, are strong evidence that entrainment was confined to a single depositional event. Similar deposits in condensed beds related to sea-level fluctuations (implying long term exposure on the sea-floor and amalgamation of several events) usually show signs of corrosion, bioerosion or abrasion (Loutit et al., 1988) and a gradational top or base (Kidwell, 1991). Furthermore, the uniformity of the background sedimentation and of the distal tempestites, and the unique occurrence of the boundary bed, without associated gradational facies or evidence of protracted reworking, oppose the interpretation that the boundary bed is a result of a relative lowering of base level owing to episodic sea-level fall. The boundary bed could be interpreted as the result of a very intense storm. This interpretation is unsatisfactory, however, because the resulting deposit was apparently untouched by subsequent storm activity, which is a climatically improbable situation for a storm-dominated setting. The unique stratigraphic occurrence of the boundary bed points to a truly exceptional erosional event, much rarer than would be expected for major storm activity.

The abundance and pyroclastic origin of the plagioclase in the sand fraction is particularly intriguing and led some authors to consider the boundary bed as a fallout tuff, dated at 66 $\pm$ 0.5 Ma on the basis of $^{40}Ar/^{39}Ar$ in a feldspar grain (Palamarczuk et al., 2002). The plagioclase age is thus only slightly older than the currently accepted 65.5 $\pm$ 0.3 Ma of the Cretaceous/Paleogene boundary (Gradstein and Ogg, 2004). The overall composition of the bed indicates that it was not directly formed by single ash fallout. The lack of pumice and the scarcity of vitreous clasts, always abundant in volcanically triggered tsunami deposits (Carey et al., 2001), also suggest that reworking in the boundary bed did not result directly from an explosive volcanic event. Concentration of plagioclase grains in the boundary bed points to reworking and winnowing of an ash bed from a pyroclastic deposit. The presence of vesicular class shards, the plagioclase zonation pattern, and the narrow range in plagioclase composition (clasts and microphenocrysts in glass shards) suggest that the plagioclase clasts and lithic clasts were derived from erosion of an andesitic pyroclastic tuff deposit that had formed during one stage of eruption of a rather homogeneous andesitic magma.

In summary, we propose the following sequence of events for the origin of the boundary bed in the Neuquén Basin (Fig. 8). Normal hemipelagic mud sedimentation in the Late Cretaceous was first interrupted by ash-fall from a distal, explosive volcanic eruption. One or several tsunami waves then caused scouring of the sea bottom

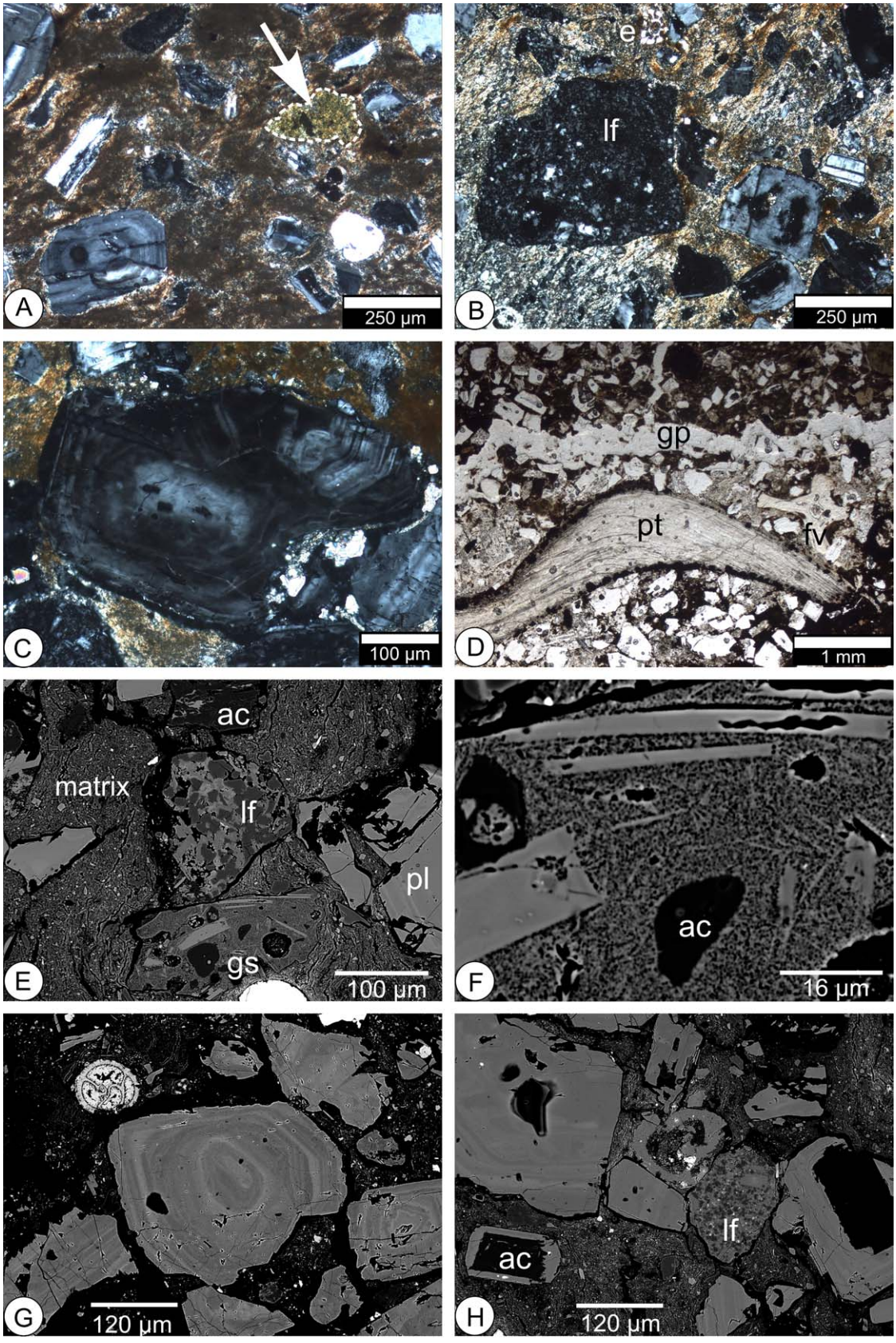
A
250 μm
B
e
lf
250 μm
C
100 μm
D
gp
pt
fv
1 mm
E
ac
matrix
lf
pl
gs
100 μm
F
ac
16 μm
G
120 μm
H
lf
ac
120 μm

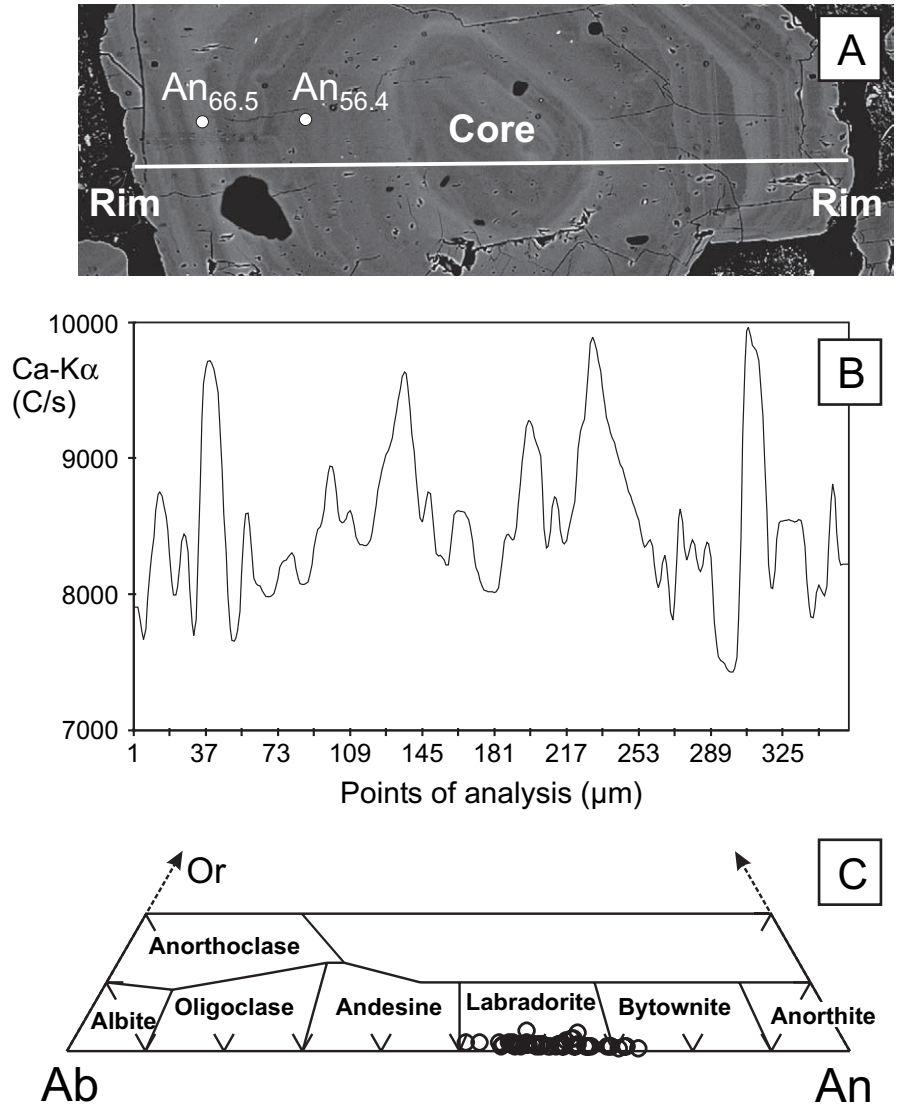

Fig. 7. Electron microprobe analyses of plagioclases of the boundary bed. A, backscattered electron image of a plagioclase clast that shows oscillatory zonation. The trace of an electron microprobe line scan analysis (360 μm) of relative Ca concentration is marked by a white line. The anorthite content derived by two quantitative point analyses is also shown. B, relative Ca concentration (Ca-Kα peak) along the profile marked in Fig. 6A, smoothed with the compound T4253H smoother of SPSS. C, plagioclase analyses (61 measurements) of 14 grains from the upper and lower part of the boundary bed plotted in a feldspar classification diagram.

and deposition of a single, normally-graded coarse-clastic bed composed of mud intraclasts, volcanic ashes and biogenic particles. Underlying muds were cracked by liquefaction of the sea bottom from secondary waves. Subsequently, normal mudstone sedimentation returned, and at the same time the bed was homogenized by intense bioturbation that extended down into the uppermost Cretaceous mudstones.

Fig. 6. Thin section micrographs (A–D) and backscattered electron images (E–H) of the boundary bed in the BJG section. A, thin section micrograph from base of boundary bed; zoned plagioclase crystals and glauconite aggregate (outlined with white stippled line and arrow) in mudstone matrix; crossed nicols. B, thin section micrograph from top of boundary bed; large lithic fragment (lf) and fragmented plagioclase crystals floating in a mudstone matrix; small echinoid spine at top of picture (e); crossed nicols. C, thin section micrograph from top of boundary bed; zoned plagioclase crystal aggregate; crossed nicols; D, thin section micrograph from base of boundary bed; pterioid bivalve shell (pt), plagioclase crystals and fish vertebra (fv) floating in a mudstone matrix. The shell is marginally impregnated by iron oxides. A young gypsum vein (gp) cuts horizontally across the bed. E, backscattered electron image from base of boundary bed; plagioclase crystal fragments (pl), lithic fragment (lf) and glass shard (gs) floating in mudstone matrix. A plagioclase almost completely replaced by analcime (ac) is located at the top of the image. F, magnification of the glass shard in E; note elongated plagioclase crystals; some vesicles are filled by analcime (ac). G, backscattered electron image from top of boundary bed; zoned plagioclase crystals and fragment of foraminifer. H, backscattered electron image from base of boundary bed; zoned plagioclase crystal fragments and lithic fragment (lf) in mudstone matrix; some plagioclase cores are replaced by analcime (ac).

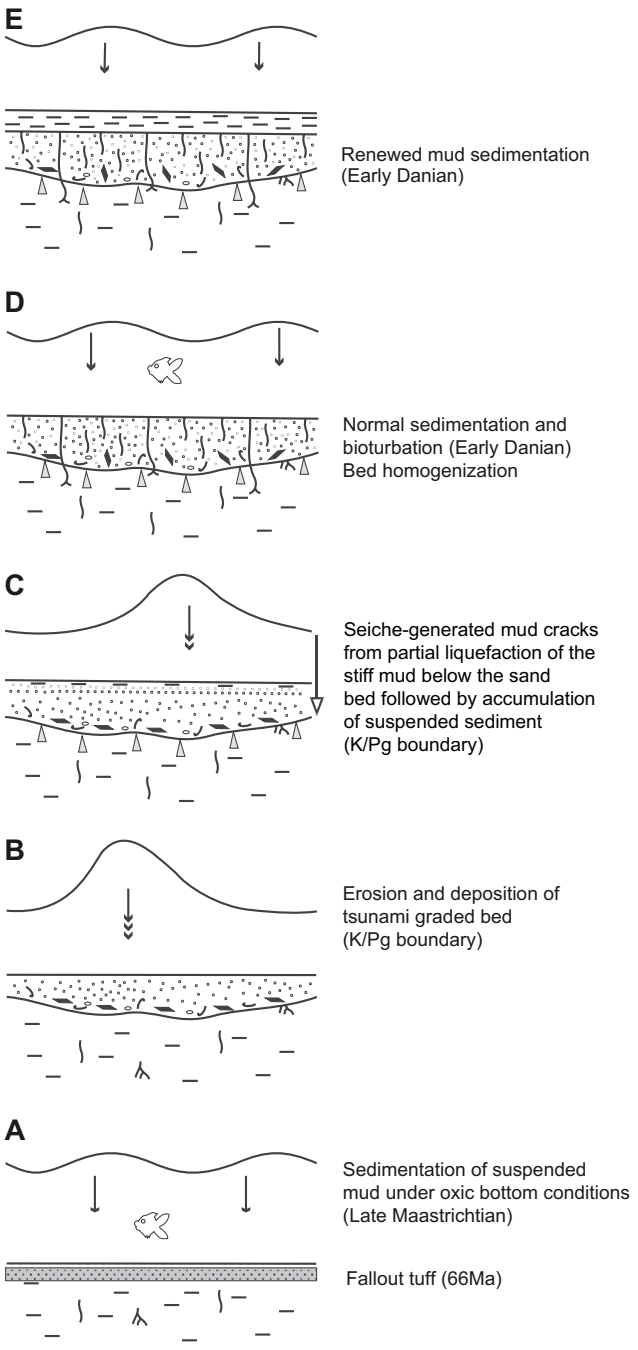

Fig. 8. A–E, model for the emplacement of the K/Pg boundary layer in the Neuquén Basin. Multiple arrow heads indicate higher sedimentation rates.

8. Discussion

The Neuquén Basin is currently the most distal K/Pg boundary site with possible indications of impact-triggered tsunami deposits. Even more distal tsunami deposits have been reported from Bjala, Bulgaria (Preisinger et al., 2002), but the tsunami origin of the boundary clay in this region is doubtful because the only evidence is minor amounts of feldspar presumably transported from coastal regions into offshore environments. At first glance, the Neuquén Basin appears to have been protected from a large tsunami originating at Chicxulub, which was approximately 7500 km distant during the latest Cretaceous. Tsunami waves, however, can travel thousands of kilometres with minimal loss of energy (Crawford and Mader, 1998). Wave heights decrease as the tsunami spreads radially from the point of origin. They are almost negligible in the open ocean, but the irregular shape of shorelines is well known to cause wave amplification during and after tsunamis and big storms (e.g. Minoura et al., 1997). The funnel-shape of the Neuquén Basin (Barrio, 1990) probably contributed substantially to the building of a high tsunami wave at this southern, mid-latitude location.

Alternatively, other large perturbations induced by the Chicxulub impact, such as seismically induced mass wasting (Norris et al., 2000; Norris and Firth, 2002; but see MacLeod et al., 2003 for criticism), could have acted as local sources of tsunami waves. Although to date only reported from the North Atlantic, there is no reason to assume that mass wasting could not have occurred in the South Atlantic as well. Our failure to detect impact tracers such as spherules, shocked quartz or an iridium anomaly in the boundary bed and the overlying mudstones cannot be explained by the distance from Chicxulub. Although ballistically transported materials (spherules, shocked quartz) are apparently not globally distributed, iridium anomalies have been recorded from all stratigraphically complete K/Pg sections, including Antarctica (Claeys et al., 2002). The absence of impact tracers and the normal terrestrial signature of trace elements in the boundary bed (Table 2) suggest that (1) the sections are slightly incomplete or (2) the impact component is strongly diluted, or (3) the tsunami deposit does not exactly coincide with the Chicxulub impact. This last possibility is suggested by the presence of a Danian nannofossil assemblage in the boundary bed. Similar observations in other regions have led some authors to postulate a Danian impact event (Koutsoukos, 1998; Stinnesbeck et al., 2002). However, in our case intense bioturbation is probably responsible for the mixture of Maastrichtian and Danian elements in the boundary bed. In any case, the tsunami interpretation is not challenged by the absence of impact tracers.

9. Conclusions

We have found a 20–25-cm-thick sandstone bed in a monotonous middle to outer shelf mudstone sequence in the Jagüel Formation. This bed is largely composed of plagioclase, mud clasts and bioclasts, and can be traced laterally for at least 5 km. Although the exact mechanisms of emplacement are poorly understood, the most parsimonious interpretation for the origin of the

Table 2
Whole-rock chemical composition of the K/Pg boundary bed and the directly overlying mudstone at the Bajada del Jagüel section (XRF analyses)

	Boundary Bed	Mudstone at BJ 30	Continental Crust[a]
Weight (%)			
SiO_2	44.3	52.3	61.5
TiO_2	0.63	0.7	0.7
Al_2O_3	18	19.5	15.1
Fe_2O_3[b]	7.79	5.02	6.3
MnO	0.06	0.08	0.1
MgO	1.54	2.09	3.7
CaO	12.8	7.08	5.5
Na_2O	2.36	2.4	3.2
K_2O	1.4	1.8	2.4
P_2O_5	0.36	0.2	0.2
SO_3	1.8	0.2	–
LOI	8.4	8.2	–
Total	99.45	99.57	98.6
[μg/g]			
Ba	384	268	584
Ce	36	49	60
Co	<15	<15	24
Cr	51	74	126
Cu	<30	<30	25
Mo	<10	<10	–
Nb	<15	<10	27
Ni	24	46	56
Pb	<15	<15	14.8
Rb	48	73	–
Sr	506	348	333
Th	<10	<10	8.5
U	<10	<10	1.7
V	115	146	98
Y	11	19	24
Zn	66	92	65
Zr	121	166	203
[ng/g]			
Ru	0.30	<0.06	0.21
	<0.06	<0.06	
Rh	0.02	<0.013	0.06
	<0.013	<0.013	
Pd	<0.13	<0.13	0.52
	0.14	0.23	
Ir	0.05	<0.04	0.02
	<0.04	<0.04	
Pt	0.31	0.08	0.51
	0.24	0.33	
Au	<0.09	<0.09	2.50
	0.18	0.31	

<Below detection limit.
LOI loss of ignition.
Samples were analysed twice for PGE.
[a] Average Continental Crust after Wedepohl (1995), Rh value after Peucker-Ehrenbrink and Jahn (2001).
[b] Total Fe as Fe_2O_3.

bed is that of a tsunami deposit related to the Chicxulub impact at the Cretaceous/Paleogene boundary. Four lines of evidence support this interpretation: (1) the rapid deposition and sedimentological criteria point to a tsunami origin; (2) nannofossil evidence of the contemporaneity of the sandstone bed with the K/Pg boundary suggests causal links between the bed and impact-related processes; (3) the presence of a "dead zone" above the sandstone bed, characterized by significantly depleted macrofossil abundances corroborates the K/Pg boundary age of the sandstone bed and underlines the ecological consequences of the K/Pg mass extinction; and (4) the stratigraphic uniqueness of the event bed within the section in terms of mineralogical composition, grain-size and sedimentary structures suggests a truly exceptional event.

The strong effect of the tsunami wave at this very distal site was probably caused by the funnel-shape of the Neuquén Basin at K/Pg boundary times, which would probably have amplified the wave considerably. Alternatively, secondary tsunami waves could have been responsible, generated by mass failure on the continental slopes of the South Atlantic. However, until such mass failure deposits are discovered, the latter explanation is speculative.

Acknowledgements

We thank the reviewers J.R. Ineson and E. Koutsoukos, whose comments led to a significantly improved manuscript. This study is funded by the Deutsche Forschungsgemeinschaft (DFG, Ki 806-1) and the Antorchas Foundation. We thank Ralf Schmitt for XRF analyses, Henning Scholz, Lucas Ruiz and Natalia Scaricabarozzi for assistance in the field, and D.J. Batten for his editorial work.

References

Aigner, T., 1985. Storm depositional systems: dynamic stratigraphy in modern and ancient shallow-marine sequences. Lecture Notes in Earth Sciences, 3. Springer, Berlin, 174 pp.

Albertão, G.A., Martins Jr., P.P., 1996. A possible tsunami deposit at the Cretaceous–Tertiary boundary in Pernambuco, northeastern Brazil. Sedimentary Geology 104, 189–201.

Alvarez, L.W., Alvarez, W., Asaro, F., Michel, H.V., 1980. Extraterrestrial cause for the Cretaceous–Tertiary extinction. Science 208, 1095–1108.

Barrio, C.A., 1990. Late Cretaceous–early Tertiary sedimentation in a semi-arid foreland basin (Neuquén Basin, western Argentina). Sedimentary Geology 66, 255–275.

Bertels, A., 1970. Los foraminíferos planctónicos de la cuenca Cretácica–Terciaria en Patagonia Septentrional (Argentina), con consideraciones sobre la estratigrafía del Fortín General Roca (Provincia de Río Negro). Ameghiniana 7, 1–47.

Bertels, A., 1975. Ostracod ecology during the Upper Cretaceous and Cenozoic in Argentina. Bulletins of American Paleontology 65, 318–388.

Bondevik, S., Svendsen, J.I., Mangerud, J., 1997. Tsunami sedimentary facies deposited by the Storegga tsunami in shallow marine basins and coastal lakes, western Norway. Sedimentology 44, 1115–1131.

Bouchette, F., Séguret, M., Moussine-Pouchkine, A., 2001. Coarse carbonate breccias as a result of water-wave cyclic loading (uppermost Jurassic–South-East Basin, France). Sedimentology 48, 767–789.

Bourgeois, J., Hansen, T.A., Wiberg, P.L., Kauffman, E.G., 1988. A tsunami deposit at the Cretaceous–Tertiary boundary in Texas. Science 241, 567–570.

Bown, P.R., Young, J., 1998. Techniques. In: Bown, P.R. (Ed.), Calcareous Nannofossil Biostratigraphy. Kluwer, Dortrecht, pp. 16–28.

Burnett, J.A., 1998. Upper Cretaceous. In: Bown, P.R. (Ed.), Calcareous Nannofossil Biostratigraphy. Kluwer, Dortrecht, pp. 132–199.

Carey, S., Morelli, D., Sigurdsson, H., Bronto, S., 2001. Tsunami deposits from major explosive eruptions: an example from the 1883 eruption of Krakatau. Geology 29, 347–350.

Carey, S., Sigurdsson, H., 2000. Grain size of Miocene volcanic ash layers from sites 998, 999, and 1000: implications for source areas and dispersal. In: Leckie, R.M., Sigurdsson, H., Acton, G.D., Draper, G. (Eds.), Proceedings of the Ocean Drilling Program, Scientific Results 165, pp. 101–113.

Cheel, R.J., Leckie, D.A., 1993. Hummocky cross-stratification. In: Wright, V.P. (Ed.), Sedimentology Review 1. Blackwell, Oxford, pp. 103–122.

Claeys, P., Kiessling, W., Alvarez, W., 2002. Distribution of Chicxulub ejecta at the KT boundary. In: Koeberl, C., MacLeod, K.G. (Eds.), Catastrophic Events and Mass Extinctions: Impacts and Beyond. Geological Society of America, Special Paper 356, 55–68.

Clague, J.J., Bobrowski, P.T., Hutchinson, I., 2000. A review of geological records of large tsunamis at Vancouver Island, British Columbia, and implications for hazard. Quaternary Science Reviews 19, 849–863.

Concheyro, A., Náñez, C., 1994. Microfossils and biostratigraphy of the Jagüel and Roca formations (Maestrichtian–Danian), Province of Neuquén. Ameghiniana 31, 397–398.

Cowan, C.A., James, N.P., 1992. Diastasis cracks: mechanically generated synaeresis-like cracks in Upper Cambrian shallow water oolite and ribbon carbonates. Sedimentology 39, 1101–1118.

Crawford, D.A., Mader, C.L., 1998. Modeling asteroid impact and tsunami. Science of Tsunami Hazards 16, 21–30.

Dawson, A.G., 1999. Linking tsunami deposits, submarine slides and offshore earthquakes. Quaternary International 60, 119–126.

Gardin, S., Monechi, S., 1998. Palaeoecological change in middle to low latitude calcareous nannoplankton at the Cretaceous/Tertiary boundary. Bulletin de la Société Géologique de France 169, 709–723.

Goff, J., Chagué-Goff, C., Nichol, S., 2001. Paleotsunami deposits: a New Zealand perspective. Sedimentary Geology 143, 1–6.

Gradstein, F.M., Ogg, J.G., 2004. Geologic Time Scale 2004 – why, how, and where next! Lethaia 37, 175–181.

Håkansson, E., Thomsen, E., 1999. Benthic extinction and recovery patterns at the K/T boundary in shallow water carbonates, Denmark. Palaeogeography, Palaeoclimatology, Palaeoecology 154, 67–85.

Hansen, T.A., Upshaw, B.I., Kauffman, E.G., Gose, W., 1993. Patterns of molluscan extinction and recovery across the Cretaceous–Tertiary boundary in east Texas: report on new outcrops. Cretaceous Research 14, 685–706.

Hayes, M.O., 1967. Hurricanes as geological agents: case studies of hurricanes Carla, 1961, and Cindy, 1963. Texas Bureau of Economic Geology, Reports of Investigations 61, 54 pp.

Henriksson, A.S., 1996. Calcareous nannoplankton productivity and succession across the Cretaceous–Tertiary boundary in the Pacific (DSDP Site 465) and Atlantic (DSDP Site 527) Oceans. Cretaceous Research 17, 451–477.

Hildebrand, A.R., Penfield, G.T., Kring, D.A., Pilkington, M., Camargo, A., Jacobsen, S.B., Boynton, W.V., 1991. Chicxulub crater: a possible Cretaceous/Tertiary boundary impact crater on the Yucatan Peninsula, Mexico. Geology 19, 867–871.

Jiang, M.J., Gartner, S., 1986. Calcareous nannofossil succession across the Cretaceous/Tertiary boundary in east-central Texas. Micropaleontology 32, 232–255.

Kidwell, S.M., 1991. Condensed deposits in siliciclastic sequences: observed and expected features. In: Einsele, G., Ricken, W., Seilacher, A. (Eds.), Cycles and Events in Stratigraphy. Springer, Berlin, pp. 682–695.

Kiessling, W., Baron-Szabo, R., 2004. Extinction and recovery patterns of scleractinian corals at the Cretaceous–Tertiary boundary. Palaeogeography, Palaeoclimatology, Palaeoecology 214, 195–223.

Kiessling, W., Claeys, P., 2001. A geographic database approach to the KT boundary. In: Buffetaut, E., Koeberl, C. (Eds.), Geological and Biological Effects of Impact Events. Springer, Berlin, pp. 83–140.

Koutsoukos, E.A.M., 1998. An extraterrestrial impact in the early Danian: a secondary K/T boundary event? Terra Nova 10, 68–73.

Loutit, T.S., Hardenbol, J., Vail, P.R., Baum, P., 1988. Condensed sections: the key to age dating and correlation of continental margin sequences. In: Wilgus, C., Hastings, B.S., Kendal, C.G., Posamentier, H.W., Ross, C.A., van Wagoner, J.C. (Eds.), Sea Level Changes – an Integrated Approach. Society of Economic Paleontologists and Mineralogists, Special Publication 42, 183–213.

MacLeod, K.G., Fullagar, P.D., Huber, B.T., 2003. $^{87}Sr/^{86}Sr$ test of the degree of impact-induced slope failure in the Maastrichtian of the western North Atlantic. Geology 31, 311–314.

Minoura, K., Imamura, F., Takahashi, T., Shuto, N., 1997. Sequence of sedimentation processes caused by the 1992 Flores tsunami: evidence from Babi Island. Geology 25, 523–526.

Molina, J.M., Ruiz-Ortiz, P.A., Vera, J.A., 1997. Calcareous tempestites in pelagic facies (Jurassic, Betic Cordilleras, southern Spain). Sedimentary Geology 109, 95–109.

Mount, J.F., Kidder, D., 1993. Combined flow origin of edgewise intraclast conglomerates: Sellick Hill Formation (Lower Cambrian), South Australia. Sedimentology 40, 315–329.

Nanayama, F., Shigeno, K., Satake, K., Shimokawa, K., Koitabashi, S., Miyasaka, S., Ishii, M., 2000. Sedimentary differences between the 1993 Hokkaido-nansei-oki tsunami and the 1959 Miyakojima typhoon at Taisei, southwestern Hokkaido, northern Japan. Sedimentary Geology 135, 255–294.

Náñez, C., Concheyro, A., 1997. Límite Cretácico-Paleógeno, Geología y Recursos Minerales del Departamento de Añelo, Provincia del Neuquén, República Argentina. Dirección Nacional del Servicio Geológico, Anales 25, 129–149.

Nelson, A.R., Shennan, I., Long, A.L., 1996. Identifying coseismic subsidence in tidal wetland stratigraphic sequences at the Cascadia subduction zone of western North America. Journal of Geophysical Research B101, 6115–6135.

Norris, R.D., Firth, J.V., 2002. Mass wasting of Atlantic continental margins following the Chicxulub impact event. In: Koeberl, C., MacLeod, K.G. (Eds.), Catastrophic Events and Mass Extinctions: Impacts and Beyond. Geological Society of America, Special Paper 356, 79–95.

Norris, R.D., Firth, J., Blusztajn, J.S., Ravizza, G., 2000. Mass failure of the North Atlantic margin triggered by the Cretaceous–Paleogene bolide impact. Geology 28, 1119–1122.

Palamarczuk, S., Habib, D., 2001. Dinoflagellate evidence of the Cretaceous–Paleogene boundary in Argentina. Geological Society of America, Abstracts with Programs, p. 33.

Palamarczuk, S., Habib, D., Olsson, R.K., Hemming, S., 2002. The Cretaceous/Paleogene (KPg) boundary in Argentina: new evidence from dinoflagellate, foraminiferal and radiometric dating. Geological Society of America, Abstracts with Programs, p. 34.

Papú, O.H., Prámparo, M.B., Náñez, C., Concheyro, A., 1999. Palinología y micropaleontología de la Formación Jagüel (Maastrichtiano–Daniano), perfil Opazo, cuenca Neuquina, Argentina. Simposio Paleógeno de América del Sur. Actas Servicio Geológico Minero Argentino, Anales 33, 17–31.

Peters, R., Jaffe, B., Gelfenbaum, G., Peterson, C., 2003. Cascadia Tsunami Deposit Database. US Geological Survey, Open-File Report 03-13, 24 pp.

Peucker-Ehrenbrink, B., Jahn, B.-M., 2001. Rhenium–osmium isotope systematics and platinum group element concentrations: loess and the upper continental crust. Geochemistry Geophysics Geosystems 2, paper 2001GC000172.

Plessen, H.-G., Erzinger, J., 1998. Determination of the platinum-group elements and gold in twenty rock reference materials by inductively coupled plasma-mass spectrometry (ICP-MS) after preconcentration by nickel sulfide fire assay. Geostandards Newsletter 22, 187–194.

Pope, K.O., 2002. Impact dust not the cause of the Cretaceous–Tertiary mass extinction. Geology 30, 99–102.

Pospichal, J.J., 1996. Calcareous nannoplankton mass-extinctions at the Cretaceous–Tertiary boundary: an update. In: Ryder, G., Fastovski, D., Gartner, S. (Eds.), The Cretaceous–Tertiary Event and Other Catastrophes in Earth History. Geological Society of America, Special Paper 307, 335–360.

Pratt, B.R., 2002. Storms versus tsunamis: dynamic interplay of sedimentary, diagenetic and tectonic processes in the Cambrian of Montana. Geology 30, 423–436.

Preisinger, A., Aslanian, S., Brandstätter, F., Grass, F., Stradner, H., Summesberger, H., 2002. Cretaceous–Tertiary profile, rhythmic deposition, and geomagnetic polarity reversals of marine sediments near Bjala, Bulgaria. In: Koeberl, C., MacLeod, K.G. (Eds.), Catastrophic Events and Mass Extinctions: Impacts and Beyond. Geological Society of America, Special Paper 356, 213–229.

Raup, D.M., Jablonski, D., 1993. Geography of end-Cretaceous marine bivalve extinctions. Science 260, 971–973.

Schultz, P.H., D'Hondt, S., 1996. Cretaceous–Tertiary (Chicxulub) impact angle and its consequences. Geology 24, 963–966.

Seguret, M., Moussine-Pouchkine, A., Raja Gabaglia, G., Bouchette, F., 2001. Storm deposits and storm-generated coarse carbonate breccias on a pelagic outer shelf (South-East Basin, France). Sedimentology 48, 231–254.

Shelly, D., 1993. Igneous and metamorphic rocks under the microscope. Chapman and Hall, London, 445 pp.

Smit, J., Montanari, A., Swinburne, N.H.M., Alvarez, W., Hildebrand, A.R., Margolis, S.V., Claeys, P., Lowrie, W., Asaro, F., 1992. Tektite-bearing deep-water clastic unit at the Cretaceous–Tertiary boundary in northeastern Mexico. Geology 20, 99–103.

Snedden, J.W., Nummedal, D., 1991. Origin and geometry of storm-deposited sand beds in modern sediments of the Texas continental shelf. In: Swift, D.J.P., Oertel, G.F., Tillman, R.W., Thorne, J.A. (Eds.), Shelf Sand and Sandstone Bodies: Geometry, Facies and Sequence Stratigraphy. International Association of Sedimentologists, Special Publication 14, 283–308.

Uliana, M.A., Biddle, K.T., 1988. Mesozoic–Cenozoic paleogeographic and geodynamic evolution of southern South America. Revista Brasileira de Geocências 18, 172–190.

Uliana, M.A., Dellapé, D.A., 1981. Estratigafía y evolución paleoambiental de la sucesión Maestrichtiano–Eoterciaria del Engolfamiento Neuquino (Patagonia Septentrional). 8° Congreso Geológico Argentino, San Luis, Actas 3, 673–711.

Varol, O., 1998. Paleogene. In: Bown, P.R. (Ed.), Calcareous Nannofossil Biostratigraphy. Kluwer, Dortrecht, pp. 200–224.

Wedepohl, K.H., 1995. The composition of the continental crust. Geochimica et Cosmochimica Acta 59, 1217–1232.